

24-26 MAY 2022
SHORT COURSES: 23 MAY 2022
KUALA LUMPUR, MALAYSIA

LEAKAGE AND DYNAMIC FORCE COEFFICIENTS FOR A STEPPED LABYRINTH SEAL AND A STEPPED POCKET DAMPER SEAL SUPPLIED WITH WET GAS

José Torres

Graduate Research Assistant
torres.jose1826@gmail.com

Luis San Andrés

Mast-Childs Chair Professor
Lsanandres@tamu.edu

Jing Yang

Senior Research Engineer
yangjing@tamu.edu

TEES Turbomachinery Laboratory
J. Mike Walker '66 Department of Mechanical Engineering
Texas A&M University
College Station, TX 77845, USA



José Torres is a MS student in the Department of Mechanical Engineering at Texas A&M University. He is currently a graduate research assistant at the turbomachinery lab working under the direction of Dr. Luis San Andrés. His research focuses on the experimental rotordynamic characterization of annular seals operating with a two-phase flow mixture. José obtained his B.S. in Aerospace Engineering at Texas A&M University in 2018, where he graduated with honors distinction. Prior to starting his MS degree, José worked in the aerospace industry with Boeing, providing manufacturing engineering support for the production of the 737 line of commercial aircrafts.



Luis San Andrés performs research in lubrication and rotordynamics, having produced advanced technologies of hydrostatic bearings for primary power cryogenic turbo pumps, squeeze film dampers for aircraft jet engines, and gas foil bearings for oil-free micro turbomachinery. Luis is a Fellow of ASME and STLE, and a member of the Industrial Advisory Committees for the Texas A&M Turbomachinery Symposia. Dr. San Andrés has educated dozens of graduate students serving the profession. Dr. San Andrés earned a MS in ME from the University of Pittsburgh and a PhD in ME from Texas A&M University. Luis has published over 260 peer reviewed papers in numerous ASME journals and conferences, including TPS and ATPS. Several papers are recognized as best in various international conferences. In 2022, Dr. San Andrés received the ASME-IGTI Aircraft Engine Technology Award for sustained personal contributions to the field.



Jing Yang received her B.S. in Thermal and Power Engineering from Huazhong University of Science and Technology, China in 2010 and Ph.D. degree in Fluid Mechanics from Peking University, China in 2017. After graduation in 2016, she worked for three years as a post-doctoral Research Associate and two years as an assistant research engineer at the TEES Turbomachinery Laboratory. Since September 2021, Jing continues at the Turbo Lab as a Senior Research Engineer. Jing Yang's research mainly focuses on the numerical prediction (computational fluid dynamics and bulk flow model) and experimental verification of the dynamic forced performance of annular pressure seals and fluid film bearings.

ABSTRACT

Industrial centrifugal compressors use annular gap seals, typically labyrinth type, to restrict process gas leakage from high-pressure regions to low-pressure regions. Currently liquid tolerant compressors enable efficient deep-sea oil and gas facilities; and seals supplied

with a two-phase flow mixture, liquid in gas (wet gas), can have a large impact on the compressor dynamic stability and mechanical efficiency. Prior research shows that pocket damper seals (PDS) provide much more effective damping than labyrinth seals (LS), albeit a one to one comparison between the two seal types for operation with a wet gas is still scarce. This lecture details experimental results for the leakage and dynamic force coefficients for a stepped shaft PDS and a stepped shaft LS. Both seals feature the same journal diameter $D = 127$ mm, seal length $L = 0.38D$, and four blades (eight 45° pockets), and slightly different clearances. The operating conditions are similar: shaft speed up to 5,250 rpm (surface speed = 35 m/s), pressure ratios (inlet/exit) = 2.5 to 4.2, and a *wet* gas composition with up to 10% in liquid volume fraction. For an inlet LVF ranging from 0 to 10%, the LS leaks more, as its step clearance is 15% larger than that of the stepped PDS. For operation with just gas (LVF=0), the LS effective clearance (C_e) is $\sim 60\%$ larger than that for the PDS. Under *wet* gas conditions (maximum inlet LVF = 6%), C_e for the PDS decreases as LVF increases, whereas C_e for the LS increases. The LS produces negligible direct stiffness (K) and effective damping (C_{eff}) compared to the force coefficients of the PDS. The excitation frequency more so than journal speed affects the K and C_{eff} of the PDS. The PDS direct damping decreases steadily with frequency while slightly increasing as the inlet LVF increases from 0 to 0.7%. For whirl frequencies below 60 Hz, the PDS direct (centering) stiffness is negative, its magnitude increasing with the liquid content. The stepped PDS exhibited subsynchronous vibrations (SSVs) for operation with a *wet* gas, and which became broadband with more liquid added. The experimental results are a reference for the engineered design of LSs and PDSs, in particular, impeller neck-ring seals in *wet* gas centrifugal compressors.

INTRODUCTION

Centrifugal compressors utilize annular gas seals to reduce excessive leakage of the working fluid from high pressure regions to low-pressure regions. Examples of such seals include interstage seals, impeller eye seals, and balance-piston seals [1]. Labyrinth seals (LSs) are the most common sealing element type in turbomachinery, though easily replaced by pocket damper seals (PDSs) that integrate partition walls separating the 360° cavities into separate “pockets” [2], as shown in Figure 1. A LS can be constructed as different configurations including tooth-on-rotor (TOR), tooth-on-stator (TOS), and as an interlocking LS with alternating TOR and TOS.

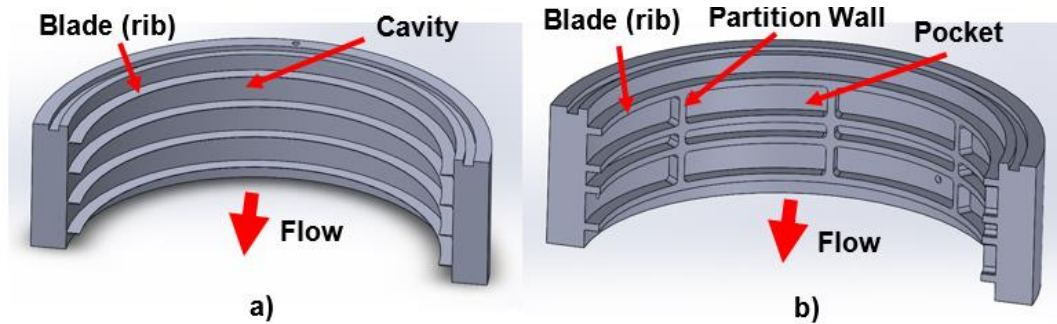


Figure 1 Illustrations of (a) labyrinth Seal (LS) and (b) fully partitioned pocket damper seal (PDS).

Labyrinth seals (LS) are a known cause of rotordynamic stability issues in shrouded compressors and turbines since their cross-coupled stiffness (k) may be large [1]. The force driving the instability is in part due to the large circumferential velocity of the gas as it enters the first tooth of the seal [1]. A practitioner may implement various modifications to remedy rotordynamic instability issues induced by LSs with the addition of swirl brakes, shunt holes and anti-swirl rings, or replacing the seal with an improved design, for example a PDS whose ability to amplify the damping coefficient (enabling more mechanical energy dissipation) is proved since nearly 30 years ago [2].

More recently, Delgado et al. (2020) [3] present comparisons of the leakage and dynamic force coefficients of a PDS versus those of a honeycomb seal (HCS) and a LS with similar physical dimensions, in particular an identical clearance $C_r = 0.20$ mm. Operating conditions with dry air include a supply pressure $P_s = 70$ bar(a), a discharge pressure $P_e/P_s = 0.25, 0.50$ and 0.65 , and rotor surface speed as high as 120 m/s (shaft speed = 20 krpm). The PDS leakage is up to 25% larger than the HCS leakage, while the LS leaks in between both. The LS produced insignificant force coefficients compared to those from the HCS and PDS, both producing a comparable effective damping coefficient (C_{eff}) and similar crossover frequencies that make $C_{eff} > 0$. The HCS produces a large direct stiffness (K), exceeding threefold the PDS stiffness. Besides manufacturing considerations, a PDS is a better alternative to a HCS whose large K may affect a compressor critical speed, hence shortening the separation margin with respect to the operating speed.

Further technological developments for subsea and offshore oil production facilities call for liquid tolerant (*wet* gas) centrifugal compressors operating under harsh conditions. The presence of liquid in a gas stream, even if in miniscule amounts, can have a large impact on the rotordynamic stability and leakage characteristics of turbomachinery. In 2014, Vannini et al. [4] conduct an in-depth investigation into the rotordynamic effects of *wet* gas ingestion into a single stage centrifugal compressor having a long LS as a balance piston. For most operating conditions, the compressor could withstand liquid content without an increase in the rotor synchronous vibration magnitudes or a change in the critical speed location. However, an unexpected sub synchronous vibration (SSV) of the rotor appeared for operation with a large flow and a liquid content up to 3% in volume. The SSV is at a frequency equaling 45% of shaft

speed and with an amplitude nearly twice that of the synchronous speed rotor motion. A root cause failure investigation revealed the SSV is closely related to the pressure drop across the balance piston along with a suspected accumulation or pooling of the liquid in the LS cavities. Replacing the LS with a fully partitioned pocket damper seal resolved the problem as the rotor SSV nearly disappeared. In the same year, to better understand the self-exciting phenomenon, Vannini et al. [5] performed an extensive CFD analysis of both a LS and PDS operating under a *wet* gas condition and learned the TOS LS is particularly sensitive to liquid entrapment within its cavities. The authors speculated the liquid circulating with a significant circumferential momentum within the LS cavities produced the instability.

During the last decade, Childs and students [6-8] at the Turbomachinery Laboratory conducted substantial experiments to quantify the leakage and force coefficients of various types of annular seals operating with a PSF-5cst silicone oil in air mixture whose LVF reached up to 10% (liquid mass fraction $\sim 57\%$). In Ref. [7], the LS has a diameter $D = 115$ mm, length $L = 0.75 D$, and radial clearance $C_r = 0.21$ mm, and operates with an inlet pressure $P_s = 62$ bar, an exit/inlet pressure ratios $(P_e / P_s) = 0.3, 0.4,$ and 0.5 and a top shaft speed of $\Omega = 15$ krpm (rotor surface speed = 90 m/s). At zero inlet pre-swirl condition, the LS direct stiffness (K) is negative for the three pressure ratios, and continues dropping with an increase in inlet LVF. The direct damping coefficient (C) linearly grows for inlet LVF $> 2\%$. At a low excitation frequency ($\omega \rightarrow 0$), the effective damping coefficient ($C_{eff} = C - k/\omega$) decreases as the inlet LVF grows, likely due to the larger cross-coupled stiffness (k) induced by the larger viscosity of the mixture. For whirl frequencies $\omega > 0.4 \Omega$, $C_{eff} > 0$ for all inlet LVFs.

In a parallel experimental program on *bubbly* liquid seals, San Andrés et al. [9-12] also report comprehensive results for the leakage and force coefficients of relatively short length seals ($L/D = 0.38$) supplied with a mixture of air in ISO VG10 oil. Applicable as eye seals in the shroud of a centrifugal pump, the test seal types included a smooth surface annular seal [10], a three-wave annular seal [11], an upstream step clearance and a downstream step clearance seal [12]. An increase in the inlet gas volume fraction (GVF) steadily reduces the mass flow through the seal and its drag torque. The seals' damping coefficient (C) is proportional to the liquid volume content; that is, C steadily increases as the GVF = $(1 - LVF)$ decreases. Note that gas content reduces the added mass coefficient typical in a liquid seal; thus producing a stiffness hardening above a certain threshold frequency even the gas volume content remains small (GVF ~ 0.05).

Moving into testing both gas and *wet* gas seals, Yang et al. (2019) [13] report measured leakage and dynamic force coefficients for a four-blade, eight-pocket PDS supplied with a mixture of air and ISO VG10 oil, with a maximum inlet LVF = 2.2% (liquid mass fraction = 84%). For an inlet LVF = 0.4% (liquid mass fraction = 57%), supply pressure $P_s = 2.3$ bar, and rotor speed $\Omega = 5,250$ rpm (rotor surface speed = 35 m/s), the direct stiffness (K) is negative and its magnitude drops with an increase in excitation frequency. Note that supplied with gas at identical P_s and Ω , the seal $K > 0.2$ MN/m. Supplied with a *wet* gas, the seal cross-coupled stiffness (k) and direct damping (C) are much greater than those under a pure gas condition. In 2021, Yang et al. [14] introduce a stepped shaft PDS that combines a conventional PDS and a rotor having two "steps" aligned with the first and third blades. The steps do not just increase the flow resistance (less leakage) but also modulate the exit of the pockets, a feature that should aid to produce more damping. Measurements conducted with both the stepped PDS and a uniform clearance (smooth surface rotor) PDS demonstrate the first seal has 1.5 times more damping than the later one. Further, the PDS direct dynamic stiffness turns negative when switching from a smooth surface journal to a stepped journal.

Besides the experimental investigations, the computational analysis of both *wet gas* and *bubbly liquid* annular seals is an ongoing effort. Both bulk-flow models (BFM) and computational fluid dynamics (CFD) models reproduce the tests seal configurations to predict the flow field under similar operating conditions; and implementing ad-hoc methods with mesh deformation along with imposed multiple-frequency shaft motions, produces the force coefficients. In 2019, San Andrés et al. [15] perform an analysis to determine the leakage, power loss, and force coefficients of a smooth surface annular seal operating with a *bubbly* liquid. The predictions corroborate the seal hardening effect, i.e., the seal dynamic stiffness (K) turning from negative to positive at a certain whirl frequency and as the GVF $> 5\%$. The stiffening effect is due to the drastic reduction in the sound speed of the mixture, even with small amounts of gas. The CFD model also predicts C_{eff} to decrease with an increase in the GVF; namely more air in the mixture reduces the viscous damping.

Recently (2021), Lu et al. [16] advance a non-homogeneous BFM for smooth surface uniform clearance seals operating with *bubbly* flow. Predictions vs. experimental data for two seals, one typical of a balance piston seal and the other one an eye-type seal, reveal the model delivers accurate direct stiffnesses (K) since it accounts for a more realistic pressure drop at the seal inlet. Yang and San Andrés [17] also introduce a simple algebraic equation model to predict the cavity pressures and leakage of both PDSs and LSs supplied with a *wet* gas. The method extends the well-known Neumann's leakage equation [18] to a *wet* gas by adapting the physical properties of a homogenous mixture. Benchmark comparisons against measured leakage and CFD predictions for two seals demonstrate the model readiness for routine engineering analyses.

Operating under a *wet* gas condition, the current work utilizes the same stepped rotor in Yang et al. [14] to further quantify the performance of a PDS vis a vis that of a similarly dimensioned LS. The experimental results will aid turbomachinery design engineers in selecting a seal type that best meets their system requirements.

EXPERIMENTAL TEST RIG AND TEST SEALS

Prior art in Refs. [9-14] provides an in-depth description of the design and operating features of the two-phase flow (wet gas) test rig shown in Figure 2. The test rig consists of a seal cartridge and a journal and rigid rotor supported on ball bearings. Four equally spaced elastic rods support the seal cartridge that hosts the test seal element, either a PDS or a LS. The top of the cartridge makes a plenum for connection to a flexible hose supplying the test seal with a mixture of pressurized oil and air. Two orthogonally positioned electromagnetic shakers and stingers deliver dynamic forces onto the cartridge to produce its motion at specific whirl frequencies and amplitude of motion.

Figure 3 presents a cross-sectional view of the test seal cartridge with the journal having a diameter $D = 2R = 127$ mm. Both the stepped PDS and the stepped LS have a total axial length $L = 48$ mm. The test seal cartridge hosts pairs of orthogonally placed piezoelectric accelerometers, eddy current displacement sensors, and dynamic load cells that measure the absolute acceleration of the seal cartridge, the relative displacement of the seal with respect to the journal, and the loads applied by the electromagnetic shakers.

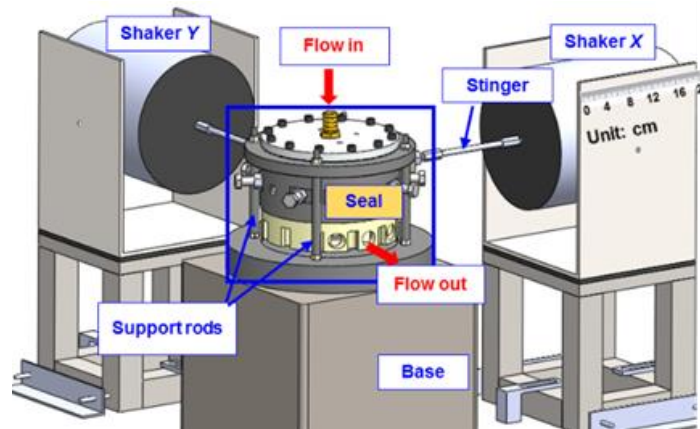


Figure 2 Schematic of wet gas seal test rig [11].

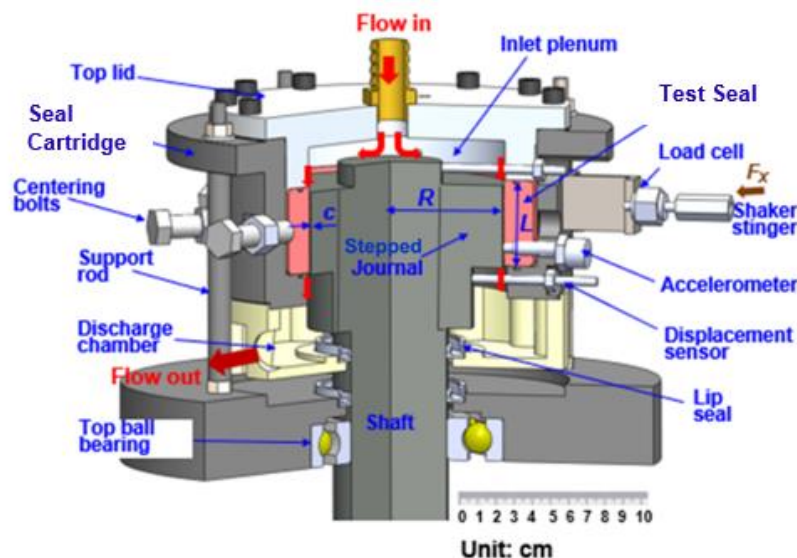


Figure 3 Cross-sectional view of seal cartridge showing the mixture flow path [11].

The test system includes separate gas and liquid lines that merge into a sparger element where the mixture is made, see Figure 4. A pump draws ISO-VG10 oil from a reservoir and moves it through a supply line. A control valve and a flow meter (range: 0.38 to 37.8 liter per minute) located downstream of the pump regulate the flow of oil. Shop dry air at a pressure of 6.9 bar(g) flows through a turbine flow meter, and after crossing a control valve that sets the gas pressure, connects to one end of the sparger. Both valves adjust the flows to achieve the desired *wet* gas mixture composition leaving the sparger and the pressure just upstream of the test seal inlet. Note the sparger is well upstream of the seal inlet. The supplied flow mixture, seen though a transparent window, shows a homogeneous mixture

with both components (liquid and gas) traveling at the same speed.

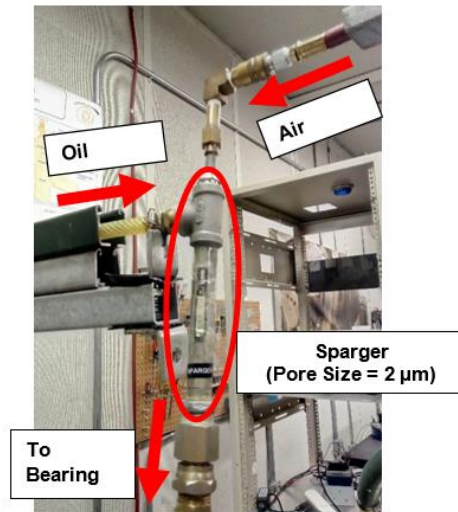


Figure 4 Sparger element mixing two separate supply lines for oil and air.

Figure 5 presents isometric and cross-sectional views illustrating the direction of flow and the seals' dimensions, also given in Table 1. The two seals have identical overall length L , journal diameter D , and cavity depth d , although featuring slightly distinct radial clearances, C_r and $C_{r,step}$, upstream and downstream of a pocket. Although designed to be identical, the clearances differ due to manufacturing error (and no budget to procure another piece). Other differences between the two seals are the thickness of the blades (ribs) and the width of the cavities/pockets. The graphs make evident the two steps machined into the journal, as in the PDS design introduced by Yang et al. [14], and whose testing demonstrated a decrease in leakage and a significant increase in direct damping when compared to a uniform clearance PDS (smooth surface rotor).

Table 1 Geometry of stepped seals (Material 6061-T6 AL).

Seal Length, L	48 ±0.03 mm		
Journal Diameter, D	127 ±0.013 mm		
	Eight-Pocket Damper Seal	Labyrinth Seal	
*Clearance, $C_{r,PDS}$	0.196 ±0.007 mm	*Clearance, $C_{r,LS}$	0.230 ±0.007 mm
*Clearance (step), $C_{r,step,PDS}$	0.106 ±0.007 mm	*Clearance (step), $C_{r,step,LS}$	0.140 ±0.007 mm
Pocket Depth, d	4.8 mm	Cavity Depth, d	4.8 mm
Pocket/Cavity Width	10.5/4.8 mm	Cavity Width	11.6 mm
Rib Width	2.5 ±0.03 mm	Tip Thickness	0.2 ±0.03 mm
Pocket Arc Length	45°	Cavity Arc Length	360°

* Measured at 21°C

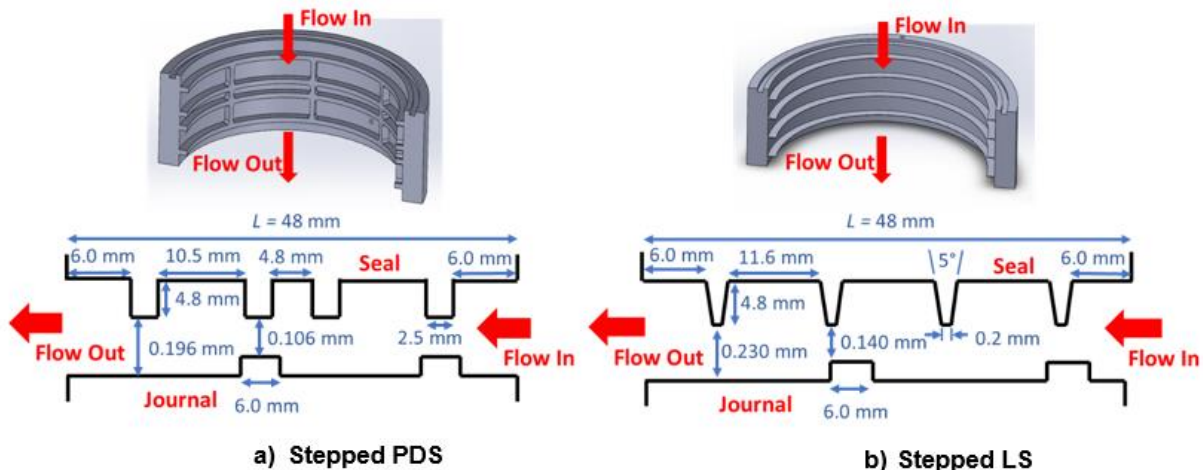


Figure 5 Diagrams illustrating dimensions of (a) stepped PDS and (b) stepped LS (not to scale).

EXPERIMENTAL PROCEDURE

Table 2 provides a summary of the fluids' physical properties and operating conditions controlled during these experiments. Measurements of seal leakage took place for a variety of operating conditions. The procedure calls to first supply air to the seal element and to measure its flow rate. Afterwards, lubricant is slowly metered to make a mixture at the desired supply pressure (P_s). The exit pressure (P_e) is ambient for all conditions.

Table 2: Lubricant properties and operating conditions.

Oil Type:	ISO-VG10
Density, ρ_{oil}	833 kg/m ³
Viscosity, μ_{oil}	15.6 cP (at 294 K)
Density, ρ_{air}	1.185 kg/m ³ at 1 bar(a), 294 K
Viscosity, μ_{air}	0.018 cP at 294 K
Mixture Supply Temp, T_s	294 K
Inlet Liquid Volume Fraction, LVF _s	0.0-0.13
Liquid Mass Fraction, LMF	0.0-0.96
Supply Pressure, P_s	2.5, 3.3, 4.2 bar(a)
Exit Pressure, P_e	1 bar(a)
Journal Speed, Ω	0, 3000, 5250 rpm
Surface Speed, $U_s = \frac{1}{2} D \Omega$	0, 19.9, 34.9 m/s

During the experiments, two flow meters record the liquid volumetric flow rate (Q_{oil}) and the gas volumetric flow ($Q_{air,s}$). Thus, the LVF of the mixture at the seal inlet equals

$$LVF_s = \frac{Q_{oil}}{Q_{oil} + Q_{air,s}} = (1 - GVF_s) \quad (1)$$

where GVF_s is the inlet gas volume fraction. Note the air flow meter displays the flow at standard conditions; hence,

$$Q_{air,s} = Q_{recorded} \left(\frac{1 \text{ bar}}{P_s} \right) \left(\frac{T_s}{289 \text{ K}} \right).$$

The mass flow rates for the oil and air equal $\dot{m}_{oil} = (\rho_{oil} Q_{oil})$ and $\dot{m}_{air} = (\rho_{air,s} Q_{air,s})$, respectively, where $\rho_{air,s} = \frac{P_s}{R_g T_s}$ is the density of air at the inlet pressure and temperature. The total leakage for the seal is then $(\dot{m}) = (\dot{m}_{air} + \dot{m}_{oil})$. Hence, the liquid mass fraction (LMF) equals

$$LMF = \frac{\dot{m}_{oil}}{\dot{m}} = (1 - GMF) \quad (2)$$

where GMF is the gas mass fraction. The LMF relates to the LVF at the seal inlet by

$$LMF = \frac{LVF_s \cdot \rho_{air,s}}{LVF_s \cdot \rho_{air,s} + (1 - LVF_s) \cdot \rho_{oil}} \quad (3)$$

Note that a $LVF_s = 5\%$ and an inlet static pressure $P_s = 2.5 \text{ bar(a)}$ corresponds to a $LMF = 94\%$; that is, small amounts of liquid in volume produce large changes to the total mass flowing through the seal. In actual practice, after recording the flow rates (Q 's) and estimating the LVF, the operator reduces the flow of air by closing the respective control valve; and afterwards, the oil flow increases until the target supply pressure (P_s) is once again achieved. The procedure of decreasing air and increasing oil is repeated until measurements take place throughout the entire range of LVF at the specified supply pressure and journal speed.

Derived from Bernoulli's Equation, the mass flow rate through the seal is a function of the pressure drop ($P_s - P_e$), the mixture density ($\bar{\rho}_m$), and the effective flow area under a tooth ($\pi D C_e$) [19]

$$\dot{m} = (\pi D C_e) \sqrt{2 \bar{\rho}_m (P_s - P_e)} \quad (4)$$

where $C_e = (c_d C_{r,step})$ is an effective clearance, with c_d denoting a fraction of the physical clearance ($C_{r,step}$). c_d is also known as a loss-like coefficient, a deviation from isentropic flow behavior. Note that for flow with just air ($LVF = 0$), $\bar{\rho}_m = \bar{\rho}_{air} = \frac{\bar{P}_m}{R_g T_s}$ with $\bar{P}_m = \frac{1}{2} (P_s + P_e)$.

For a mixture of oil and air, the average mixture density is

$$\bar{\rho}_m = \overline{\text{LVF}} \rho_{oil} + (1 - \overline{\text{LVF}}) \bar{\rho}_{air} \quad (5)$$

where $\overline{\text{LVF}} = \frac{1}{2}(\text{LVF}_s + \text{LVF}_e)$ is an average LVF. Note the exit LVF is [17]:

$$\text{LVF}_e = \frac{P_s \cdot \text{LVF}_s}{P_s \cdot \text{LVF}_s + (1 - \text{LVF}_s) P_e} \quad (6)$$

Lastly, the flow rate (\dot{m}) of the *wet* gas can be written as

$$\dot{m} = c_d (\pi D C_{r,step}) \sqrt{2 \bar{\rho}_m (P_s - P_e)} = c_d \dot{m}_{ideal} \quad (7)$$

Thus, c_d relates the measured (\dot{m}) to the ideal flow rate (\dot{m}_{ideal}) through a single-restriction seal. c_d quantifies the effectiveness of a seal to reduce leakage; a lower c_d denotes a more effective seal.

Identification of Dynamic Force Coefficients

With a mixture of oil and air flowing through the seal and the rotor spinning at a set speed (Ω), a shaker applies a unidirectional periodic load $\mathbf{F}_x = [f_x = f_o e^{i\omega t}, f_y = 0]^T$ to the seal cartridge. Here, f_o and ω denote the load amplitude and its frequency as recorded by the load cell. The accelerometers record the ensuing cartridge accelerations $\mathbf{A}_x = [A_{xx}, A_{yx}]^T$, and the eddy-current sensors record the seal cartridge displacements $\mathbf{D}_x = [X_x, Y_x]^T$ relative to the journal. The data acquisition system records the time domain data \mathbf{F}_x , \mathbf{D}_x , and \mathbf{A}_x , for a total of 1 s with a sampling rate of 16,834 samples/s. Immediately after, the procedure repeats for a unidirectional periodic load applied along the Y -direction, $\mathbf{F}_y = [f_x = 0, f_y = f_o e^{i\omega t}]^T$ and the sensors record $\mathbf{A}_y = [A_{xy}, A_{yy}]^T$ and $\mathbf{D}_y = [X_y, Y_y]^T$ over a similar elapsed time.

San Andrés [20] explains the procedure for identifying the dynamic force coefficients of a two-degree of freedom mechanical system. First, the Discrete Fourier Transform of the recorded time domain records brings the data into the frequency domain. That is, let $\underline{\mathbf{F}}_{x(\omega)} = \text{DFT}(\mathbf{F}_x)$, $\underline{\mathbf{D}}_{x(\omega)} = \text{DFT}(\mathbf{D}_x)$, and $\underline{\mathbf{A}}_{x(\omega)} = \text{DFT}(\mathbf{A}_x)$. The procedure makes the matrices

$$\underline{\mathbf{F}}_{(\omega)} = [\underline{\mathbf{F}}_{x(\omega)} \mid \underline{\mathbf{F}}_{y(\omega)}], \underline{\mathbf{D}}_{(\omega)} = [\underline{\mathbf{D}}_{x(\omega)} \mid \underline{\mathbf{D}}_{y(\omega)}], \underline{\mathbf{A}}_{(\omega)} = [\underline{\mathbf{A}}_{x(\omega)} \mid \underline{\mathbf{A}}_{y(\omega)}] \quad (8)$$

The system complex dynamic stiffness \mathbf{H} at frequency (ω) follows as

$$\mathbf{H}_{(\omega)} = [\underline{\mathbf{F}}_{(\omega)} - M_{sc} \underline{\mathbf{A}}_{(\omega)}] \underline{\mathbf{D}}_{(\omega)}^{-1} \quad (9)$$

Where $M_{sc} = 14$ kg is the mass of the seal cartridge and the installed seal. Note that \mathbf{H} superimposes the contributions from both the seal and the test rig elastic structure

$$\mathbf{H}_{(\omega)} = \mathbf{H}_{\text{Seal}(\omega)} + \mathbf{H}_{\text{Structure}(\omega)} \quad (10)$$

$\mathbf{H}_{\text{Structure}}$ is first identified from performing dynamic load tests with the dry (non-lubricated) system at ambient pressure. The test rig structure has a support stiffness $K_S = 3.77$ MN/m, a natural frequency of ~ 82.6 Hz, and a (sizeable) damping ratio equal to ~ 0.06 . Excitation frequencies around 80 Hz are not exerted during the dynamic load tests.

Lastly, the test seal complex stiffness (\mathbf{H}_{Seal}) follows from

$$[\mathbf{H}_{(\omega)} - \mathbf{H}_{\text{Structure}(\omega)}] = \mathbf{H}_{\text{Seal}(\omega)} \rightarrow \mathbf{K}_{(\omega)} + i \omega \mathbf{C}_{(\omega)} : \begin{bmatrix} H_{xx} & H_{xy} \\ H_{yx} & H_{yy} \end{bmatrix} = \begin{bmatrix} K_{xx} & K_{xy} \\ K_{yx} & K_{yy} \end{bmatrix} + i \omega \begin{bmatrix} C_{xx} & C_{xy} \\ C_{yx} & C_{yy} \end{bmatrix} \quad (11)$$

Above the real part corresponds to the seal stiffness \mathbf{K} and the imaginary part is proportional to the damping coefficients \mathbf{C} . The seal element is assumed to provide identical principal or direct stiffnesses, $H_{xx} = H_{yy} = (K + i \omega C)$, and asymmetric cross stiffnesses, $H_{xy} = -H_{yx} = (k + i \omega c)$. Lastly, the seal effective damping coefficient equals

$$C_{eff} = C - k/\omega = [\text{Ima}(H_{xx}) - \text{Real}(H_{xy})]/\omega \quad (12)$$

EXPERIMENTAL RESULTS

The figures below depict direct comparisons of the leakage (\dot{m}) for both seals supplied with an oil in air mixture. The effective clearance (C_e) quantifies the effectiveness of both seals to restrict leakage. Next, the direct stiffness (K) and the effective damping coefficient (C_{eff}) depicted vs. the excitation frequency (ω) provide a comparison of the seals' rotordynamic performance.

Leakage for stepped PDS and LS

Operating with just air ($LVF_s = 0$), Figure 6 depicts the leakage (\dot{m}) and the effective clearance (C_e) for both PDS and LS vs. the (supply/exit) pressure ratio and three shaft speeds. Note \dot{m} is insensitive to journal speed, since the flow axial velocity is likely greater than the circumferential velocity. For example, for the PDS operating with $(P_s/P_e) = 1.32$ and at the top journal speed of 5,250 rpm, the rotor surface speed $U_s = 34.9$ m/s whereas the smallest recorded axial speed $U_a = 87$ m/s. The largest Reynolds number $Re = \frac{\rho_{air,exit} U C_{r,step}}{\mu_{air}}$, with U as the fluid speed, ranges from 650 to 1,900 as $(P_s/P_e) = 1.3$ to 2.6.

In physical magnitude, the stepped PDS shows a lower leakage than the LS. The distinct clearances at the steps, 0.106 mm for the PDS vs 0.140 mm for the LS, explain the differences in leakage. For both seals note the effective clearance (C_e) is relatively constant for most pressure ratios $(P_s/P_e) > 1.4$. The data produces $C_{e,PDS} = 0.041$ mm = $0.387C_{r,step,PDS}$, and $C_{e,LS} = 0.068$ mm = $0.486C_{r,step,LS}$. Note the ratio of effective clearance to physical clearance, $c_d = (C_e/C_r)$, is known as a loss-like coefficient that evidences the effectiveness of the seal to deducing the leakage. Hence, for the current data, the PDS is a more effective seal than the LS is.

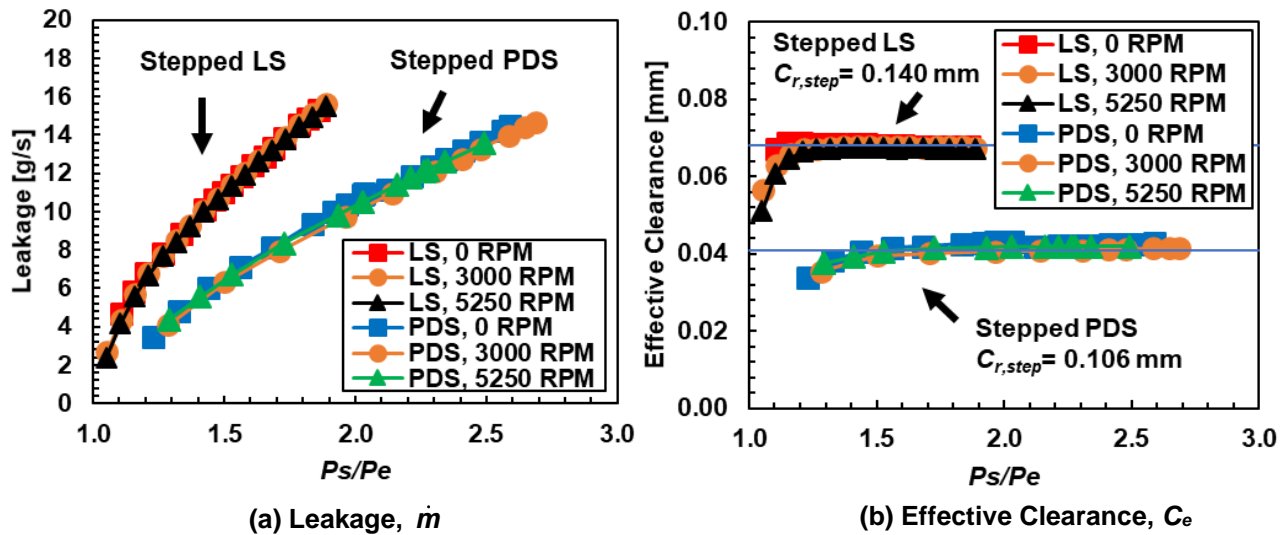


Figure 6 Leakage (\dot{m}) and effective clearance (C_e) vs. pressure ratio (P_s/P_e) for a stepped PDS and a stepped LS operating with air. Journal speed = 0, 3,000, and 5,250 rpm.

For operation without journal speed ($\Omega = 0$) and with pressure ratio $(P_s/P_e) = 2.56$, Figure 7 shows the leakage (\dot{m}) and effective clearance (C_e) vs. the mixture inlet LVF. Note that for $LVF_s = 5\%$, the liquid mass fraction = 94%. As expected, both seals leak more as the LVF_s increases since the density of the oil is orders of magnitude larger than that of the supplied air, i.e., $(\rho_{oil}/\rho_{air}) = 290$ at $P_s = 2.5 P_e$. Again, the stepped LS leaks more because of its larger clearances. The seals' effective clearance (C_e) offers differing trends for both seals. The C_e for the LS increases as the liquid content increases and is larger than the magnitude obtained for pure gas condition, $C_{e,LS} = 0.068$ mm. On the other hand, the stepped PDS shows a $C_e (< 0.041$ mm) decreasing steadily as the liquid content increases. Hence, the effectiveness of the LS to restrict the leakage of a liquid in gas mixture decreases, whereas that of the PDS increases. Besides having a smaller clearance at the steps ($C_{r,PDS}/C_{r,LS} = 0.71$), the PDS leaks less *wet* content as likely liquid pools in the pockets; same as reported in Ref. [5].

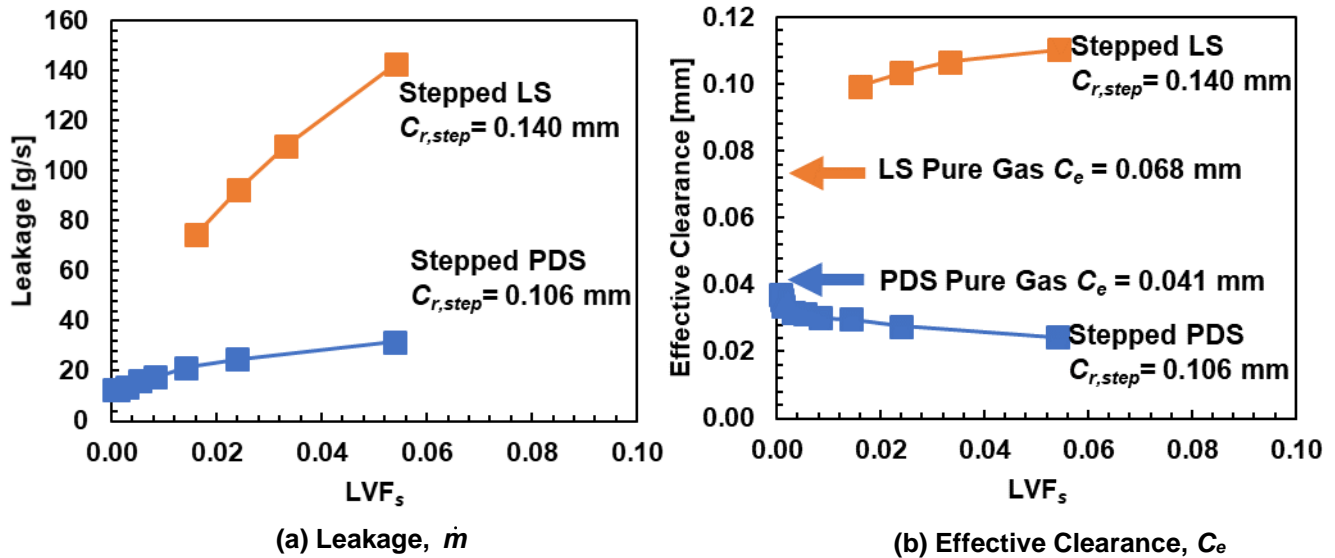


Figure 7 Leakage (\dot{m}) and effective clearance (C_e) vs. inlet LVF for a stepped PDS and a stepped LS. Journal speed = 0 rpm and pressure ratio (P_s/P_e) = 2.56.

Figure 8 depicts the PDS leakage (\dot{m}) vs. LVF_s for operation at three pressure ratios, $P_s/P_e = 2.56, 3.34,$ and $4.2,$ and three journal speeds = 0, 3,000, and 5,250 rpm. Note the journal speed has a small influence on the seal leakage that quickly increases with both the supplied pressure and the liquid content in the mixture. Figure 9 shows the PDS effective clearance (C_e) vs. pressure ratio (P_s/P_e) and operation at two journal speeds. Each graph contains data for two or more LVFs, the largest shown being 6.4%. Recall $C_{e,PDS} = 0.041$ mm for the pure gas condition, and one immediately notes that C_e decreases as the liquid content increases.

The uncertainty in leakage measurements for both seals comprises the contributions from the individual uncertainties for the air and oil flow meters, 0.3% and 2.0% of the measured value, respectively. Thus, the total uncertainty in the measurement of *wet* gas leakage is ~2.02% of the measured value.

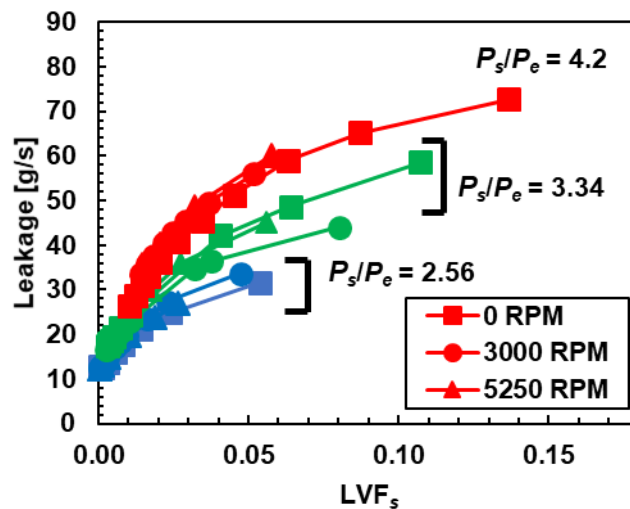


Figure 8 Stepped PDS: Leakage (\dot{m}) vs. inlet LVF for operation at three journal speeds and three supply pressures (max. 5,250 rpm and $P_s/P_e = 4.2$).

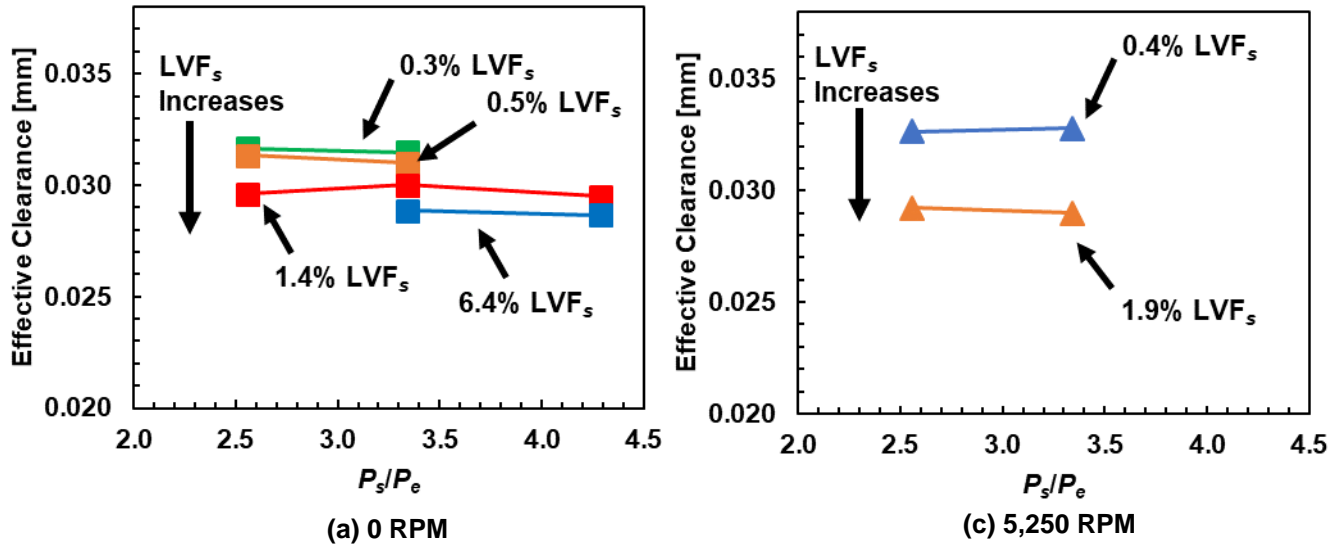


Figure 9 Stepped PDS: Effective clearance (C_e) vs. pressure ratio (P_s/P_e) for operation at journal speeds = (a) 0 and (b) 5,250 rpm. Inlet LVF varies from 0.3% to 6.4%.

Dynamic Force Coefficients for PDS and LS

Figure 10 presents the seals' identified direct stiffness (K) and effective damping (C_{eff}) vs. excitation frequency. In the experiments, the pressure ratio $P_s/P_e = 2.35$ and the mixture LVF_s = 1.3%. The journal speed is 0 and 5,250 rpm (rotor surface speed = 35 m/s). In the graphs, a vertical dashed line denotes the frequency synchronous with shaft speed.

Koo [21] details the calculation of uncertainty for dynamic force coefficients identified with the method leading to Eq. (8). The total uncertainty adds precision and bias uncertainties. Each measurement, conducted no less than three times, establishes a precision uncertainty with a 95% confidence interval. The cross-coupled force coefficients for both seals are very small in magnitude, difficult to quantify with accuracy. The bias uncertainty for K and C_{eff} are $U_K = 4.6\%$ and $U_C = 5.9\%$ of the identified parameter magnitude, respectively. The following figures depicting the force coefficient depict the total uncertainty as error bars in the respective graph.

In short, the stepped LS provides minuscule force coefficients, K and C_{eff} , compared to those from the pocket damper seal. The stepped PDS offers an effective damping (C_{eff}) that decreases with excitation frequency albeit with a magnitude slightly increasing as the journal speed increases. It is interesting to realize that the stepped PDS offers a negative direct stiffness ($K < 0$) at frequencies below 60 Hz. The largest negative stiffness for the stepped PDS is -1.67 MN/m for the case with journal speed = 5,250 rpm and excitation frequency = 10 Hz. Note that the magnitude of the negative stiffness is about 45% of the magnitude of the support stiffness, $K_s = 3.77$ MN/m, thus causing a 25% decrease in system natural frequency.

Prior experimental work reports the leakage and force coefficients for the uniform clearance PDS [13] and the stepped shaft PDS [14] supplied with pure gas. The current experimental results reproduce those in Ref. [14] for operation without shaft speed ($\Omega = 0$). Having a smaller clearance, the stepped PDS leaks ~ 50% less and produces more damping. The increase in C is 50% to 150% as ($P_s/P_e = 2.3 \rightarrow 3.2$). For the stepped PDS supplied with pure gas and no shaft speed ($\Omega = 0$) [14], the experimental $K < 0.5$ MN/m for $P_s/P_e = 2.3$ over a wide frequency range (20 Hz ~ 120 Hz), whereas the direct damping (C) decreases with frequency.

For operation of the PDS with oil in air mixtures of increased LVF content, Figure 11 depicts the force coefficients, K and C_{eff} vs. frequency and operation with pressure ratio (P_s/P_e) = 2.5. Regardless of the magnitude of journal speed (0 and 5,250 rpm), the results showcase that, depending on the magnitude of the excitation frequency, increasing the amount of liquid does affect the direct stiffness (K). At low whirl frequencies ($\omega < 80$ Hz), $K < 0$ and turns more negative as the inlet LVF increases. K remains relatively impervious to the liquid content at high whirl frequencies ($\omega \rightarrow 150$ Hz). The trends outlined above are similar to those reported by Zhang and Childs [8] for a honeycomb seal supplied with inlet LVF from 0 to 7%. Increasing the liquid content in the mixture tends to increase the effective damping (C_{eff}), likely due to the higher viscosity of the two-component fluid flow. Note that C_{eff} quickly decreases with excitation frequency.

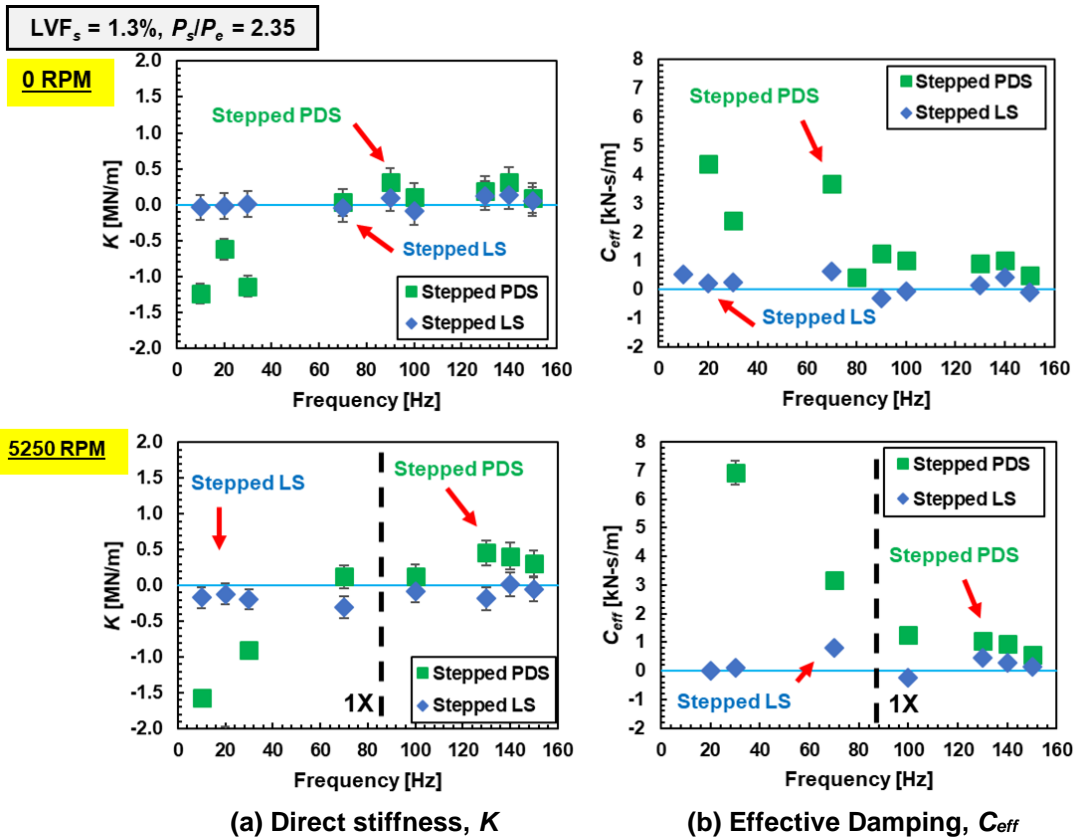


Figure 10 Stepped LS and PDS: Direct stiffness (K) and effective damping (C_{eff}) vs. excitation frequency. Operation with $P_s/P_e = 2.35$, inlet LVF = $1.3\% \pm 0.05\%$, and three journal speeds (0 and 5,250 rpm).

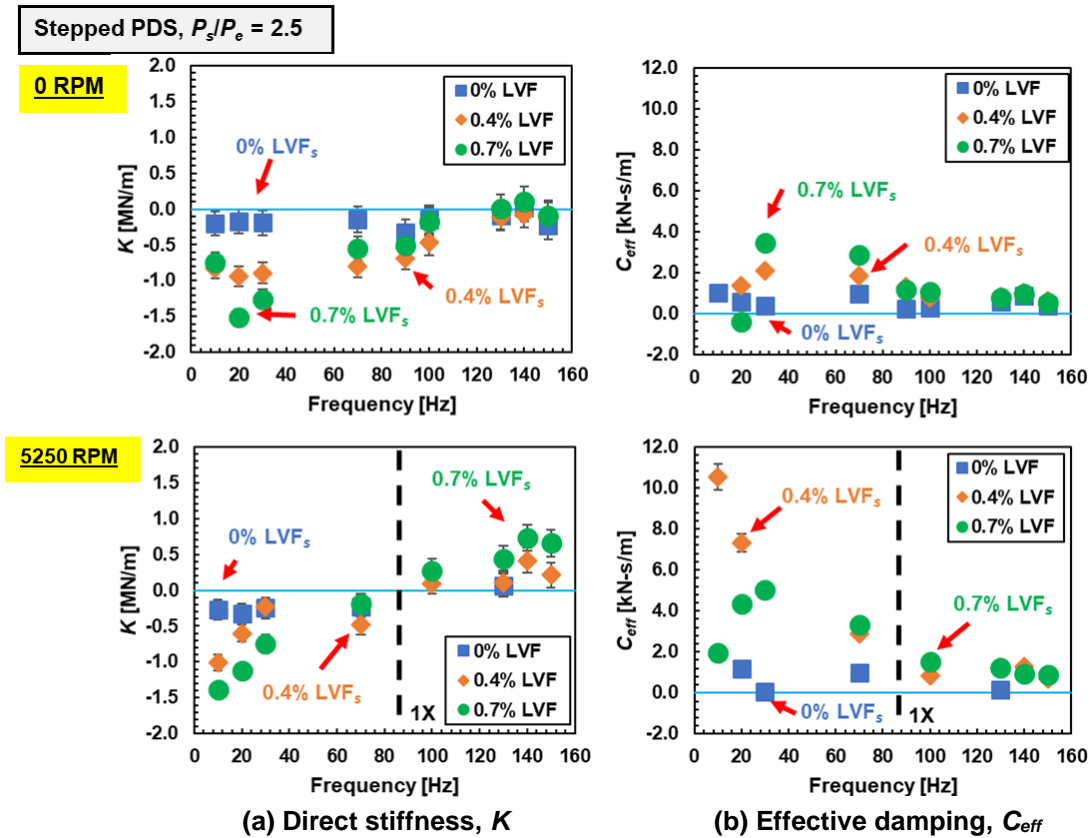


Figure 11 Stepped PDS: Direct stiffness (K) and effective damping (C_{eff}) vs. excitation frequency. Operation with $P_s/P_e = 2.5$, inlet LVF varies = (0, 0.4, 0.7)%, and two journal speeds (0 and 5,250 rpm).

Recorded Subsynchronous Vibrations of Seal Cartridge

Vannini et al. [4] document unexpected rotor subsynchronous vibrations (SSV) during operation of a LS supplied with wet gas LS whose LVF_s ranged from 0% to 3%. The SSV frequency equaled 45% of shaft speed and its amplitude was nearly twice that of the shaft speed motion. The reference documents a broadband SSV frequency spectrum exacerbated by the presence of liquid content. Interestingly enough, the same phenomenon did not occur with a PDS replacing the LS.

Figure 12 presents surface plots illustrating the amplitude and frequency of the cartridge motions when operating both seals, LS and PDS, while stepwise varying the liquid content in the two-phase flow mixture during an elapsed time of 60 s. The LVF_s ranged from 2.7% to 1.3% for the stepped LS, and LVF = 2.5% to 0.1% for the stepped PDS. The measurements, conducted without any dynamic load excitation, reveal the cartridge holding the stepped LS mainly shows vibrations synchronous with shaft speed. On the other hand, unexpectedly as per the prior art described in Ref. [4], the cartridge hosting the PDS reveals broadband SSV motions worsening as the liquid content increases. The maximum amplitude of the SSVs is small ($\approx 5 \mu\text{m}$) compared to the amplitude of synchronous shaft speed motions ($\approx 38 \mu\text{m}$). Note the color scale in Figure 12 ranges from 0 to $5 \mu\text{m}$ to better illustrate the SSVs, thus it does not apply to the synchronous speed motions. The SSV motions decrease in amplitude and disappear as the LVF decreases (more gas is added).

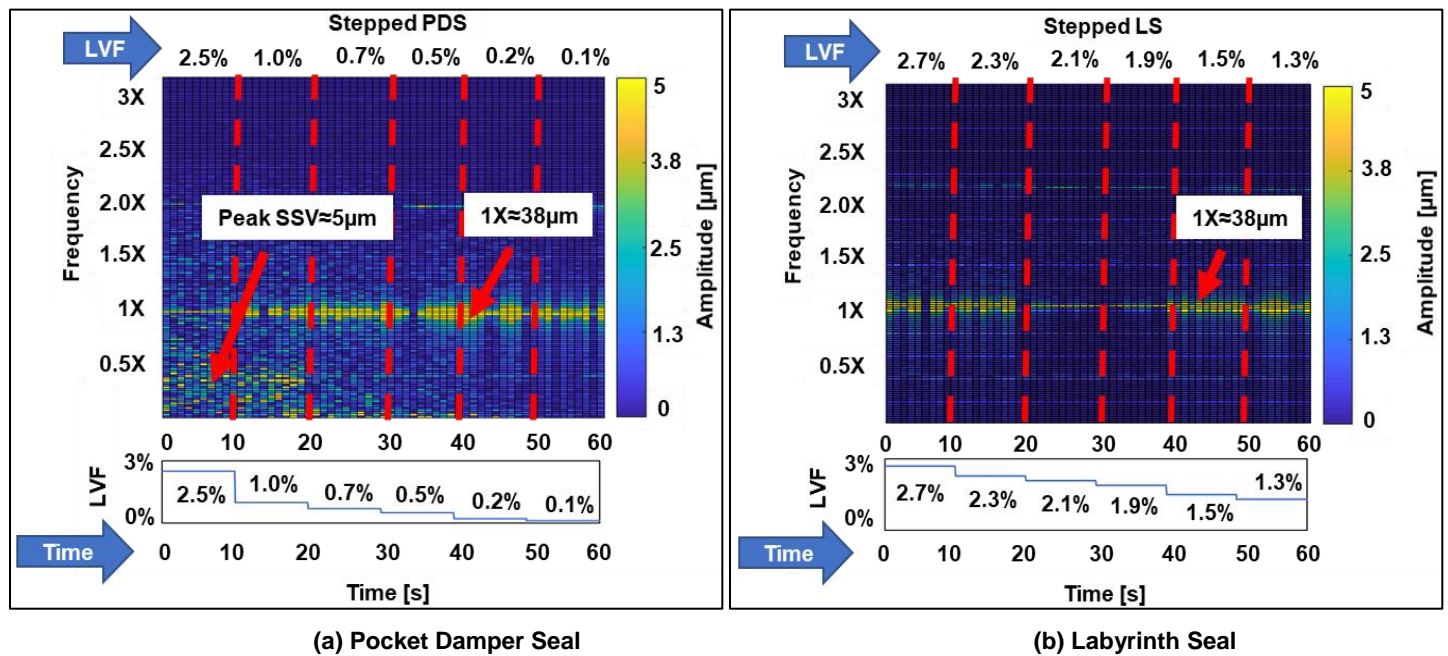


Figure 12 Stepped PDS and LS: Amplitude and frequency of subsynchronous vibration vs. time and inlet LVF. Journal speed = 3000 RPM (50 Hz) and pressure ratio (P_s/P_e) = 2.5.

San Andrés and Lu [11] report a similar self-excited broadband SSV occurring for a smooth annular seal operating with a two-phase flow with a LVF < 80%. Contrary to the present results, the authors in [11] observe an increase in amplitude and broadband frequency content as the GVF increases (liquid content decreases), although operation with just air caused the excitation to suddenly disappear. The authors argue the self-excited SSVs are related to the sound speed of the mixture being too low, thus producing an acoustic resonance. Presently, however, the SSV found with the PDS supplied with a liquid in gas mixture is likely due to the seal negative direct stiffness appearing at low excitation frequencies.

CONCLUSIONS

The lecture presents the leakage and force coefficients of a stepped shaft pocket damper seal (PDS) and a stepped shaft labyrinth seal (LS) operating with a *wet* gas made of an oil in air mixture. The two seals share the same rotor diameter, axial length, and number of blades or ribs, albeit differing in radial clearance due to a manufacturing error. The experiments were conducted with the seals operating under similar conditions in supply pressure, inlet liquid volume fraction (LVF_s) and journal rotational speed. The major findings are:

- Supplied with pure gas, the PDS leakage is smaller than that for the LS; hence the pocket damper seal has a smaller effective clearance (C_e). Note $C_e/C_{r,step} = 0.387$ for the PDS vs. $C_e/C_{r,step} = 0.486$ for the LS for all journal speeds and inlet pressure conditions, hence denoting the PDS is more effective in restricting leakage.

- (b) Supplied with a two-phase flow, as the LVF_s increases, the effective clearance (C_e) of the stepped PDS decreases whereas the one for the LS increases significantly.
- (c) When supplied with the same inlet pressure and LVF_s, the PDS produces a much larger effective damping (C_{eff}) than the stepped LS does for all excitation frequencies. The PDS shows a negative direct stiffness ($K < 0$) for low frequency excitation, while the LS produces virtually a null centering stiffness. The larger the liquid content, the larger its effect on the direct stiffness and damping of the PDS. That is, as the LVF increases so does the magnitude of the direct damping and stiffness, albeit $K < 0$ for frequencies below 60 Hz.
- (d) The leakage and effective clearance (C_e) of both seals is insensitive to shaft speed due to the larger axial flow velocity of the mixture compared to its circumferential flow velocity. The effective damping (C_{eff}) of the stepped PDS tends to increase slightly in magnitude as the shaft speed increases whereas the C_{eff} of the stepped LS remains of the same magnitude. The direct stiffness (K) of both seals shows an insensitivity to shaft speed.
- (e) The stepped PDS produces unexpected broadband subsynchronous vibrations (SSVs) of the test cartridge and that increase in amplitude as the LVF_s of the *wet* gas increases. The SSVs are absent in tests with the stepped LS. The SSVs could be a result of the negative direct stiffness ($K < 0$) of the stepped PDS at low excitation frequencies, thus producing a deviation of the seal displacement from its centered position.

Comparisons of the current experimental results, namely leakage and dynamic force coefficients, vs. predictions (CFD and bulk flow models) are currently in progress.

NOMENCLATURE

C_e	Seal effective clearance [m]
C_{eff}	$(C - k / \omega)$. Seal effective damping coefficient, [N-s/m]
c_d	$(C_e / C_{r,step})$. Seal leakage loss coefficient or fraction of physical clearance [-]
C, c	Direct and cross-coupled ($i \neq j$) damping coefficients [N/m]
C_r	Nominal clearance [m]
$C_{r,step}$	Clearance at step location [m]
D	Journal diameter [m]
H_{ij}	Direct ($i = j$) and cross-coupled ($i \neq j$) complex stiffnesses [N/m]
K, k	Direct and cross-coupled stiffnesses [N/m]
K_s	Structure stiffness [3.77 MN/m]
L	Seal axial length [m]
\dot{m}	Mass flow rate [kg/s]
M_{sc}	Mass of seal and its cartridge [14 kg]
P_s	Supply pressure [Pa]
P_e	Exit (discharge) pressure [Pa]
\bar{P}_m	$\frac{1}{2}(P_s + P_e)$, mean pressure [Pa]
Q_{air}	Volumetric flow rate [m ³ /s]
R_G	Air gas constant [J/(kg-K)]
T_s	Supply temperature [K]
U_s	$\frac{1}{2} \Omega D$. Journal surface speed [m/s]
μ	Fluid viscosity [cP]
ρ	Fluid density [kg/m ³]
ω	Excitation (whirl) frequency [rad/s]
Ω	Journal speed [rad/s]

Vectors and Matrices

A	Seal cartridge acceleration
D	Seal cartridge displacement
F	Load applied to seal stator
H	Complex dynamic stiffness matrix

Abbreviations

GVF	Gas volume fraction
GMF	Gas mass fraction
LMF	(1 – GMF). Liquid mass fraction

LS	Labyrinth seal
LVF	(1 – GVF). Liquid volume fraction
PDS	Pocket damper seal
SSV	Subsynchronous vibrations

Subscripts

<i>air</i>	Air (gas)
<i>e</i>	Exit
<i>m</i>	Mixture or two-phase flow
<i>oil</i>	Oil (liquid)
<i>s</i>	Supply/Inlet

Superscript

–	Arithmetic mean value
---	-----------------------

ACKNOWLEDGMENT

The financial support and interest of the Turbomachinery Research consortium (TRC) at Texas A&M University are gratefully acknowledged.

REFERENCES

- [1] Childs, D.W., and Vance, J. M., 1997, “Annular Gas Seals and Rotordynamics of Compressors and Turbines,” Proc. of the 26th Turbomachinery Symposium, Houston, TX, September 16-18, pp. 201-220. <https://doi.org/10.21423/R1HT06>.
- [2] Vance, J. M., and Schultz, R. R., 1993, “A New Damper Seal for Turbomachinery,” Proc. of the 14th Biennial Conference on Mechanical Vibration and Noise, Albuquerque, NM, September 19-22, pp 139-148. <https://doi.org/10.1115/DETC1993-0188>.
- [3] Delgado, A., San Andrés, L., Thiele, J., Yang, J., and Cangioli, F., 2020, “Rotordynamic Performance of a Fully-Partitioned Damper Seal: Experimental and Numerical Results,” Proc. of the 49th Turbomachinery and the 36th Pump Symposium, Virtual, December 07-11, <https://turbolab.tamu.edu/proceedings/>.
- [4] Vannini, G, Bertoneri, M., Del Vescovo, G., and Wilcox, M., 2014, “Centrifugal Compressor Rotordynamics in Wet Gas Conditions,” Proc. of the 43rd Turbomachinery Symposium, Houston, TX, September 22-25, pp. 201-220. <https://doi.org/10.21423/R1F93J>.
- [5] Vannini, G., Bertoneri, M., Nielsen, K. K, Ludiciani, P., and Stronach, R., 2016, “Experimental Results and Computational Fluid Dynamics Simulations of Labyrinth and Pocket Damper Seals for Wet Gas Compression,” ASME J. Eng. Gas Turbines Power, **138**(5), pp. 052501. <https://doi.org/10.1115/1.4031530>.
- [6] Zhang, M., Mclean, J. E., and Childs, D. W., 2017, “Experimental Study of the Static and Dynamic Characteristics of a Long Smooth Seal with Two-Phase, Mainly Air Mixtures,” ASME J. Eng. Gas Turbines Power, **139**(12), pp. 122504. <https://doi.org/10.1115/1.4037607>.
- [7] Shrestha, H., Childs, D. W., Tran, D. L., and Zhang, M., 2019, “Experimental Study of the Static and Dynamic Characteristics of a Long (L/D= 0.75) Labyrinth Annular Seal Operating under Two-Phase (Liquid/Gas) Conditions,” ASME J. Eng. Gas Turbines Power, **141**(11), pp. 111002. <https://doi.org/10.1115/1.4044309>.
- [8] Zhang, M., and Childs, D. W., 2020, “A Study for Rotordynamic and Leakage Characteristics of a Long-Honeycomb Seal with Two-Phase, Mainly Air Mixtures,” ASME J. Eng. Gas Turbines Power, **142**(1), pp. 011021. <https://doi.org/10.1115/1.4044947>.
- [9] San Andrés, L., Lu, X., and Liu, Q., 2016, “Measurements of Flow Rate and Force Coefficients in a Short-Length Annular Seal Supplied with a Liquid/Gas Mixture (Stationary Journal),” Tribol. Trans., **59**(4), pp. 758–767. <https://doi.org/10.1080/10402004.2015.1102370>.
- [10] San Andrés, L., and Lu, X., 2017, “Leakage, Drag Power and Rotordynamic Force Coefficients of an Air in Oil (Wet) Annular Seal,” ASME J. Eng. Gas Turbines Power, **140**(1), pp. 012505. <https://doi.org/10.1115/1.4037622>.
- [11] San Andrés, L., and Lu, X., 2018, “Leakage and Rotordynamic Force Coefficients of a Three-Wave (Air in Oil) Wet Annular Seal: Measurements and Predictions,” ASME J. Eng. Gas Turbines Power, **141**(3), pp. 032503. <https://doi.org/10.1115/1.4041270>.
- [12] San Andrés, L., Lu, X., and Jie, Z., 2018, “On the Leakage and Rotordynamic Force Coefficients of Pump Annular Seals Operating with Air/Oil Mixtures: Measurements and Predictions,” Second Asia Turbomachinery and Pump Symposium, The Turbomachinery Laboratory, Texas A&M University, Singapore, Mar. 13–15. <https://hdl.handle.net/1969.1/175007>.
- [13] Yang, J., San Andrés, L., Lu, X., 2019, “Leakage and Dynamic Force Coefficients of a Pocket Damper Seal Operating Under a

- Wet Gas Condition: Tests Versus Prediction,” ASME J. Eng. Gas Turbines Power, **141**(11), pp. 111001. <https://doi.org/10.1115/1.4044307>.
- [14] Yang, J., San Andrés, L., Lu, X., 2021, “On the Leakage and Dynamic Force Coefficients of a Novel Stepped Shaft Pocket Damper Seal: Experimental and Numerical Verification,” ASME J. Eng. Gas Turbines Power, **143**(3), pp. 031002. <https://doi.org/10.1115/1.4048459>.
- [15] San Andrés, L., Yang, J., and Lu, X., 2019, “On the Leakage, Torque, and Dynamic Force Coefficients of Air in Oil (Wet) Annular Seal: A Computational Fluid Dynamics Analysis Anchored to Test Data,” ASME J. Eng. Gas Turbines Power, **140**(2), pp. 021008. <https://doi.org/10.1115/1.4040766>.
- [16] Lu, X., San Andrés, L., and Yang, J., 2021, “A Nonhomogeneous Bulk Flow Model for Gas in Liquid Flow Annular Seals: an Effort to Produce Engineering Results,” ASME J. Tribol. (in print), <https://doi.org/10.1115/1.4052678>.
- [17] Yang, J., and San Andrés, L., 2021, “An Analytical Two-Phase Flow Model for Prediction of Leakage in Wet Gas Labyrinth Seals and Pocket Damper Seals. Is Simplicity Still Desired?” ASME J. Eng. Gas Turbines Power, **143**(12), pp. 121016. <https://doi.org/10.1115/1.4051916>.
- [18] Childs, D. W., 1993, *Turbomachinery Rotordynamics: Phenomena, Modeling, and Analysis*, Chapter 5, “Rotordynamic Models for Annular Gas Seals,” John Wiley & Sons, New York, NY.
- [19] San Andrés, L., Wu, T., Barajas-Rivera, J., Zhang, J., and Kawashita, R., 2019, “Leakage and Cavity Pressures in an Interlocking Labyrinth Gas Seal: Measurements Versus Predictions,” ASME J. Eng. Gas Turbines Power, **141**(10), pp 101007. <https://doi.org/10.1115/1.4044284>.
- [20] San Andrés, L., 2009, *Modern Lubrication Theory*, “Experimental Identification of Bearing Force Coefficients,” Notes 14, Texas A&M University Digital Libraries, [Mar 30, 2020], <http://oaktrust.library.tamu.edu/handle/1969.1/93254>, [accessed April 2021].
- [21] Koo, B., 2019, “Experiments and Models for Operation of a Sealed Ends Squeeze Film Dampers: A Step Towards Quantifying Air Ingestion in Squeeze Films,” Ph.D. dissertation, Texas A&M University, College Station, TX.